2015

Refining late Quaternary plunge pool chronologies in Australia's monsoonal 'Top End'

Jan-Hendrik May
University of Wollongong, hmay@uow.edu.au

Frank Preusser
Stockholm University, frank.preusser@natgeo.su.se

Luke A. Gliganic
University of Wollongong, lukeg@uow.edu.au

Publication Details

May, J., Preusser, F. & Gliganic, L. Andrew. (2015). Refining late Quaternary plunge pool chronologies in Australia's monsoonal 'Top End'. Quaternary Geochronology, 30 (Part B), 328-333.

Refining late Quaternary plunge pool chronologies in Australia's monsoonal 'Top End'

Abstract
Plunge pool deposits from Australia's 'Top End' are considered as important archives of past monsoonal activity in the region. The available chronology of these deposits was so far based on thermoluminescence (TL) dating and indicated maximum flood magnitudes during the Last Glacial Maximum in contrast with more arid conditions as deduced from other archives of the region. This study revisits plunge pool deposits at Wangi Falls by applying multiple and single-grain Optically Stimulated Luminescence (OSL) dating of quartz and high-resolution gamma spectrometry, supported by radiocarbon dating of organic material. The aim is to reappraise the existing chronology and investigate if the deposits are affected by partial bleaching, post-depositional mixing and/or problems related to annual dose determination. The latter seems to have a minor impact on the ages at most. Equivalent Dose (De) distributions are broad, in particular for single grains, but apparently not result from partial bleaching or post-depositional mixing. Rather, microdosimetry caused by radiation hotspots in the sediment and zircon inclusions in the quartz grains is considered problematic for these sediments. The results presented here imply that the previous TL chronology overestimated the real deposition age of the sediments.

Disciplines
Medicine and Health Sciences | Social and Behavioral Sciences

Publication Details
May, J., Preusser, F. & Gliganic, L. Andrew. (2015). Refining late Quaternary plunge pool chronologies in Australia's monsoonal 'Top End'. Quaternary Geochronology, 30 (Part B), 328-333.

Refining late Quaternary plunge pool chronologies in Australia's monsoonal 'Top End'

Jan-Hendrik May[1,3*], Frank Preusser[2,3], Luke Andrew Gliganic[1,4]

[1] *GeoQuest and Wollongong Isotope Geochronology Lab, School of Earth and Environmental Sciences, University of Wollongong, Australia*

[2] *Department of Physical Geography and Quaternary Geology, Stockholm University, 10691 Stockholm, Sweden*

[3] *Present address: Institute of Earth and Environmental Sciences - Geology, University of Freiburg, Albertstr. 23b, 79104 Freiburg, Germany*

[4] *Present address: Institute of Geology and Palaeontology, Leopold-Franzens University of Innsbruck, Innrain 52, 6020 Innsbruck, Austria*

* Corresponding author: janhendrikmay@googlemail.com

Abstract

Plunge pool deposits from Australia's 'Top End' are considered as important archives of past monsoonal activity in the region. The available chronology of these deposits was so far based on thermoluminescence (TL) dating and indicated maximum flood magnitudes during the Last Glacial Maximum in contrast with more arid conditions as deduced from other archives of the region. This study revisits plunge pool deposits at Wangi Falls by applying multiple and single-grain Optically Stimulated Luminescence (OSL) dating of quartz and high-resolution gamma spectrometry, supported by radiocarbon dating of organic material. The aim is to reappraise the existing chronology and investigate if the deposits are affected by partial bleaching, post-depositional mixing and/or problems related to annual dose determination. The latter seems to have a minor impact on

the ages at most. Equivalent Dose (D_e) distributions are broad, in particular for single grains, but apparently not result from partial bleaching or post-depositional mixing. Rather, microdosimetry caused by radiation hotspots in the sediment and zircon inclusions in the quartz grains is considered problematic for these sediments. The results presented here imply that the previous TL chronology overestimated the real deposition age of the sediments.

Keywords: *OSL dating, quartz, microdosimetry, monsoon, Australia*

1. Introduction

Today, Australia's 'Top End' (the northernmost section of the Northern Territory) is dominated by a highly monsoonal climate (Fig. 1), with fluvial systems characterized by strong seasonal flood dynamics related to cyclone activity. Late Holocene variability in flood magnitudes and frequencies are directly related to the strength of the Australian Summer Monsoon (ASM) and its modulation by El Niño Southern Oscillation (ENSO). In contrast, our understanding of ASM variability, its main controls over longer timescales, and the impact of large-scale hydrological changes on the environment and fluvial systems is limited. Recently, an increasing number of site specific high-resolution datasets from Australasia have suggested mostly dry conditions during the Last Glacial Maximum (LGM, ca. 20 ka ago) with the return of the monsoon not before ca. 15 ka (Reeves et al., 2013). However, the only available terrestrial dataset from the 'Top End' is based on proximal flood sediments associated with waterfall plunge pools (Nott et al., 1996; Nott and Price, 1999), suggesting significantly increased flooding frequencies and magnitudes during the LGM. This interpretation is in conflict to the notion of an overall weakened monsoon during glacial times, but

crucially relies on the accuracy of the thermoluminescence (TL) based chronology, which might be affected by two principal problems that have not been fully addressed in previous publications. Firstly, determination of Equivalent Dose (D_e) using a TL multiple-grain approach could have been affected by partial bleaching and/or post-depositional mixing, which could eventually lead to both over- and underestimation of depositional ages. Secondly, Nott et al. (1996) explain the apparent underestimation of some ages by the passage of soluble uranium salts within the water table that could have affected certain parts of the sediment body. However, their application of thick source alpha counting for dose rate determination did not allow to further investigate this issue nor check for radioactive disequilibrium.

In this study, we have re-sampled plunge pool flood sediments in Litchfield National Park with the aim of assessing, refining and improving the plunge pool chronology at Wangi Falls (Fig. 1), and thereby test the validity of existing interpretations. Optically Stimulated Luminescence (OSL) multi-grain aliquot and single-grain dating of quartz in combination with high-resolution gamma spectrometry and ICP-MS are applied to overcome the technical limitations of previous studies. The four main objectives of this study are (i) to assess the possibility of dose rate related problems such as radioactive disequilibrium and uranium dissolved in groundwater, (ii) to investigate if partial bleaching and/or post-depositional mixing are affecting the sediments in a proximal waterfall setting, (iii) to test if the existing TL chronology is supported by radiocarbon and OSL dating, and finally (iv) to determine the most likely depositional ages for the flood sediments.

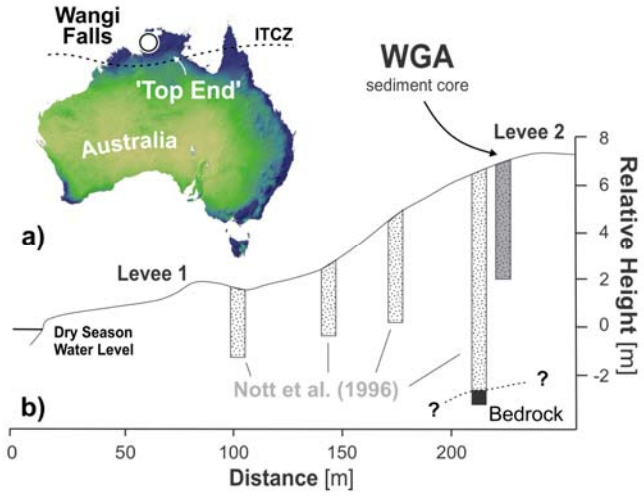

Fig. 1: Location map: a) Overview map Australia, b) cross-section levee sample location.

2. Methodology

2.1. Sampling

Sediment cores down to 5 m depth were extracted in opaque plastic liners with a motor driven manual percussion corer from the crest of the flood levee at Wangi Falls (core WGA, 13.1631°S/130.6817°E; Fig. 1). The cores were subsequently opened in a red-light laboratory and sampled for OSL dating (STable 1). For this, sediment was taken from ca. 6 cm thick portions in the centre of the cores, whereas surrounding material was sampled for dose rate determination. To assess the potential effects of partial bleaching on D_e distributions, two additional samples were collected as modern analogues from Wangi Creek immediately after the flood season in April 2014; WG-Bar comes from a submerged bar at ca. 80 cm below water surface in the waterfall plunge pool, WG-552 from a subaerial bar associated with high-velocity flows immediately downstream of the plunge pool.

After sampling for OSL, all cores were described with regard to their stratigraphical and sedimentological characteristics (i.e. colour, grain size, angularity, organic material, charcoal) to establish a stratigraphic framework and identify material from hole collapse in the upper parts of the cores. Thin sections from each successive meter down-core were prepared from the in-situ sediment. Their micromorphological analysis encompassed their visual inspection under a polarization microscope, and the quantification of the main sedimentary constituents by point counting (see Supplementary Material). Sediment was sampled from 15 different depths, weighed, and then dried and weighed at 50°C and 450°C, respectively, in order to estimate field moisture and organic content (Loss on Ignition, LOI). Finally, organic layers and macroscopic charcoal were sampled for radiocarbon dating. Charcoal and organic material was prepared for standard AMS radiocarbon dating at Beta Analytics (US) and the University of Waikato (New Zealand) by washing in hot HCl, rinsing and treating with multiple hot NaOH washes. Then, the NaOH insoluble fraction was treated

with hot HCl, filtered, rinsed and dried, to eliminate potential effects of contamination by younger humic acids. The resulting radiocarbon ages were calibrated using Calib 7.0 (Stuiver and Reimer, 1993) and the SHcal13 calibration curve (Hogg et al., 2013).

2.2. OSL sample preparation and measurement set-up

The ca. 65 km^2 catchment area of Wangi Creek exclusively contains quartzite, sandstone, and minor lateritic lithologies (Ahmad et al., 1993), and visual inspection confirmed that the sediment consists almost entirely of quartz grains. Therefore, we used a simplified preparation technique including sieving (160-250 µm and 180-212 µm), chemical pre-treatment with H_2O_2 to eliminate organic matter, and HF treatment (40 % for one hour, followed by 15 % HCl). Heavy minerals such as zircon are of much smaller grain size than used for quartz extraction and will hence not contaminate the samples. For multi-grain aliquot analyses, 2 mm of the surface of the sample carrier discs were covered with a thin film of silicon oil using a stamp. Measurements were performed using a Freiberg Instruments Lexsyg Research reader (Richter et al., 2013). Each disc was exposed to IR LDs (850 nm, 350 mW cm^{-2}, at 50°C) to check for feldspar contamination but none showed any response. OSL was recorded at 125°C during a 60 s exposure to blue LEDs (emission 458 nm, 60 mW cm^{-2}) using the combination of a Hoya U-340 (2.5 mm) and a Delta-BP 365/50 EX-Interference as detection filter (5 mm) and an Electron Tubes Ltd 9635Q photomultiplier. The initial 0.4 s minus the final 10 s subtracted as background were used for signal integration. For single-grain measurements, grains were loaded into mircohole discs and were stimulated with green (532 nm) laser light for 2 s at 125°C in a Risø DA20 TL/OSL reader (Bøtter-Jensen et al., 2003). D_e values were estimated by summing the first 0.17 s of signal and using the final 0.3 s as background. The ultraviolet OSL emissions were measured using an Electron Tubes Ltd 9635Q photomultiplier tube fitted with a 7.5 mm Hoya U-340 filter. Laboratory irradiations were given using calibrated $^{90}Sr/^{90}Y$ beta sources attached to the readers.

The Single Aliquot Regenerative Dose (SAR) protocol has been applied and dose recovery experiments were used to assess the appropriateness of various preheat combinations, suggesting that most combinations are suitable for D_e estimation in the low dose range considered here (SFig. 1). Preheats of 230°C for 10 s preceded all multi-grain aliquot OSL measurements (natural, regenerative, and test dose). Applying these preheat combinations we also performed paired multi-grain aliquot analysis on three samples to ensure reproducibility between laboratories and machines, and found excellent agreement (SFig. 2). For single-grain measurements, preheats of 230°C for 10 s and 180°C for 10 s preceded natural/regenerative and test dose measurements, respectively. For each sample at least 25 multi-grain aliquots and 500 individual grains were measured. Standard rejection criteria such as natural test dose signals and errors, recycling ratios, and a recuperation test were applied to both multi- and single-grain aliquots (STable 2; Murray and Wintle, 2000). An OSL-IR depletion ratio (Duller, 2003) was also applied for single-grain measurements.

Determination of dose rate relevant elements (K, Th, U) was carried out by high-resolution gamma spectrometry (cf. Preusser and Kasper, 2001). Investigation for radioactive disequilibrium was done as explained in Zander et al. (2007), by using the activity determined for different isotopes of the uranium decay chain (^{238}U, ^{226}Rn, ^{210}Pb; STable 3). In addition to the sediments, the concentration of dose relevant elements has also been determined for a laterite, sandstone, and quartzite sample from the surroundings of Wangi Falls. Present day depth was used for the calculation of cosmic dose rate following Prescott and Hutton (1994). As cores were taken at the end of the tropical dry season, and groundwater tables are subject to strong oscillations over various timescales, the calculation of dose rate assumed that the average water content during burial was between 4 and 12 %. To estimate a potential effect of radioactive elements dissolved in groundwater passing through the sediments, we measured water samples from Wangi Falls (WG-Falls) and a spring which drains the quartzite escarpment and flows into the plunge pool (WG-437) using an Inductively Coupled Plasma-Mass Spectrometer (ICP-MS; Supplementary Methods).

3. Results

3.1. Stratigraphy and sediments

Based on sedimentary characteristics two main stratigraphic units are distinguished in the core. The upper 200 cm below the ground are composed of greyish to brownish fine to medium sands with some granules, whereas the remaining 300 cm down to 5 m are characterized by alternating whitish fine to medium sands, pinkish coarse angular gravel up to several cm in diameter, and horizontal mm to cm thick beds of black, charcoal rich organic material with > 1% LOI (Fig. 2). A well-developed soil has formed in the upper 200 cm and is also reflected in the gradually decreasing moisture and LOI values down-profile. Microscopical analysis of thin sections from the original sediment confirmed that quartz is the dominating mineral, but also reveals the presence of partly iron rich mud pellets of different size and shape at ca. 0.2-0.5 counts per mm^2 (Fig. 3a, b; STable 4). Also, the analysis revealed varying quantities of heavy mineral grains in the sediment at ca. 0.04-0.4 counts per mm^2, but additional heavy minerals (e.g. zircon) are present as inclusions in many quartz grains (Fig. 3c, d). Radiocarbon dating yielded stratigraphically consistent ages between ca. 15.3 and 18.8 cal. ka BP in the lower half of the core (STable 5). At ca. 38 cm below surface, a charcoal fragment returned a pMC value of >100 and is essentially modern.

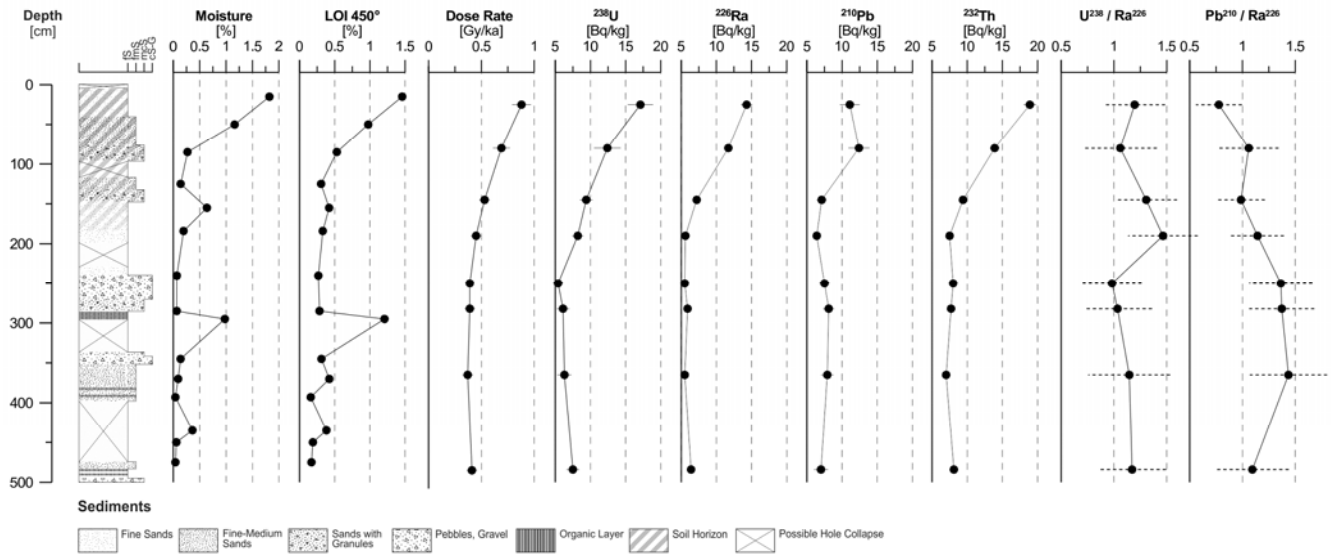

Fig. 2: Core WGA at Wangi Falls with main stratigraphic and sedimentary characteristics, and down-profile variation in moisture, LOI, total dose rate, ^{238}U, ^{226}Ra, ^{210}Pb, ^{232}Th, $^{238}U/^{226}Ra$, and $^{210}Pb/^{226}Ra$ (note: uncertainties on ratios are 2σ).

The concentration of radioactive elements and hence the dose rates for the sediments are generally low, and range between ca. 0.35 Gy ka^{-1} and ca. 0.9 Gy ka^{-1} (STable 3). In particular the concentration of K is very low and reaches not more than 0.08 %, hence only a few percent of what is usually found in sediments. This is explained by the low abundance of radioactive elements in the sandstone and quartzite of the region (STable 3). Interestingly, there is a clear trend for higher concentration of all radioactive elements in the upper part of the core, coinciding with increased organic content (LOI, Fig. 2). This is likely explained by soil formation and the laterite sample actually shows significantly higher concentrations in both uranium (18x) and thorium (9x) compared to the bedrock samples. U/Ra ratios suggest the presence of disequilibrium in two samples (WGA-II-45, WGA-II-90; Fig. 2), but only at 1-sigma level. As ^{232}Th and ^{226}Ra show very similar down-profile trends, it is unlikely that there has been a loss of radium. This may indicate that these samples could have been subject to post-depositional enrichment in uranium, possibly caused by oscillating ground water tables in the past. However, end member scenarios of uranium up-take (i.e. entire up-take at present or directly after deposition) lead to only a 10 % difference in ages. As a more continuous up-take appears more likely, the uncertainty related to this issue might not exceed a few percent and appears hence negligible in the present context (cf. Preusser and Degering, 2007). A different kind of disequilibrium, enrichment of ^{210}Pb, is observed in the lower of the core (WGA-III-50, WGA-III-82, WGA-IV-65; Fig. 2). This could reflect the degassing of ^{222}Rn, and the subsequent enrichment of daughter products (e.g. ^{210}Pb), but a significant loss of radium is not likely. Considering this and the short half-life of ^{210}Pb (22 years), a significant effect on ages appears also unlikely.

The results from ICP-MS measurements on water from the spring and from Wangi Falls show very low values close to or even below detection limit (STable 6), suggesting that the effect of dissolved U in groundwater in the sediment is minimal even at the end of the dry season.

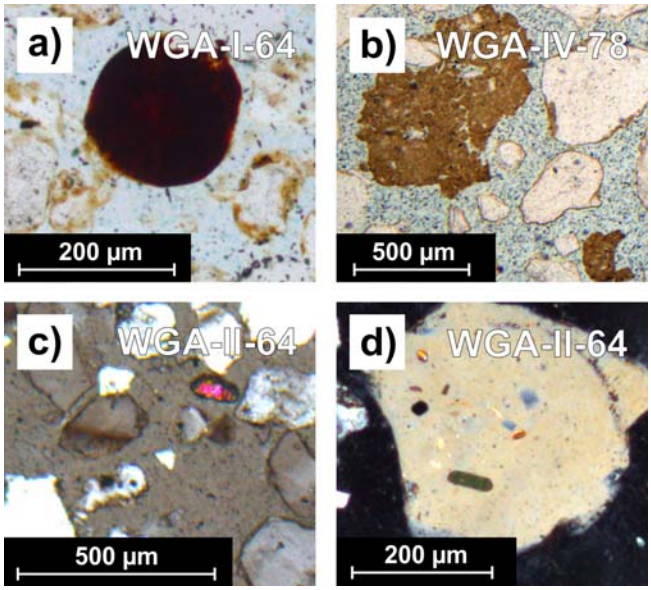

Fig. 3: Thin section photographs of a) lateritic mud-pellet (NPL), b) clay rich mud-pellet (NPL), c) unspecified detrital heavy mineral grains (XPL), and d) inclusions of unspecified heavy minerals in quartz grain (XPL).

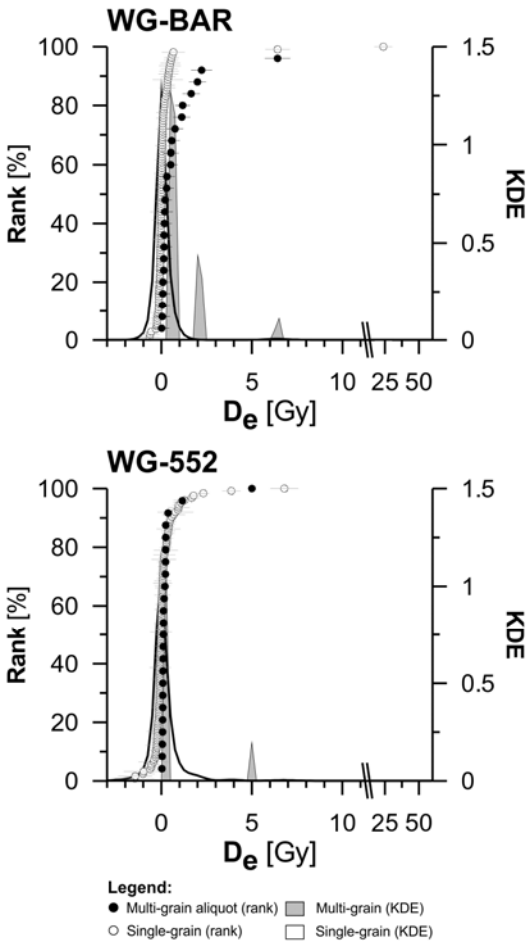

Fig. 4: Age-rank and kernel-density-estimate (KDE) plots for D_e distributions (closed circles, grey-shaded curve = multi-grain aliquots; open circles and white curve = single-grains) measured for two samples from the modern plunge pool (WG-Bar) and creek bed (WG-552).

3.3. Analyses of D_e distributions

The multi-grain aliquot and single-grain D_e data for modern samples collected from Wangi Creek are presented in Figure 4; most D_e values are centred around 0 Gy. The weighted mean D_e estimates from multi-grain aliquots for WG-Bar and WG-552 are 0.24 ± 0.08 Gy and 0.10 ± 0.03 Gy, respectively. While the presence of many negative and near-zero D_e values in the single-grain datasets prevented the calculation of standard statistical measures (i.e., Central Age Model - CAM and overdispersion), the individual D_e values support the multi-grain aliquot results. Of the individual

grains producing D_e values, 97% and 90% of grains from samples WG-Bar and WG-552, respectively, yield D_e values consistent with 0 at 2σ (Fig. 4). This is further supported by unlogged-CAM (Arnold et al., 2009) mean D_e estimates of 0.019 ± 0.002 Gy for WG-Bar, and 0.15 ± 0.76 Gy for WG-552 (STable 1). Together, these results indicate that partial bleaching during transport and deposition is not significant in the modern creek in proximity to Wangi Falls, and is therefore likely not affecting D_e estimates and ages for OSL-derived chronologies.

Grains comprising single-grain D_e distributions from the WGA core have good overall OSL properties with ca. 12-28% of grains passing all applied selection criteria (SFig. 3; STable 2). D_e distributions from the upper one meter (WGA-I-25 and I-80) have generally large spreads in D_es, with overdispersion values of 57% and 14% for multi-grain aliquots, and 80% and 57% for single grains (Fig. 5, SFig. 4; STable 1). Samples from below the uppermost meter have generally low overdispersion values (7–17% for multi-grain aliquots, and 20–36% for single grains), showing no relationship with depth. In combination with the stratified nature of the deposits this suggests that post-depositional disturbance is insignificant for samples below WGA-I. By contrast, the large spread in D_e data and the proximity to the modern surface strongly suggests that sediments in WGA-I have experienced significant post-depositional mixing.

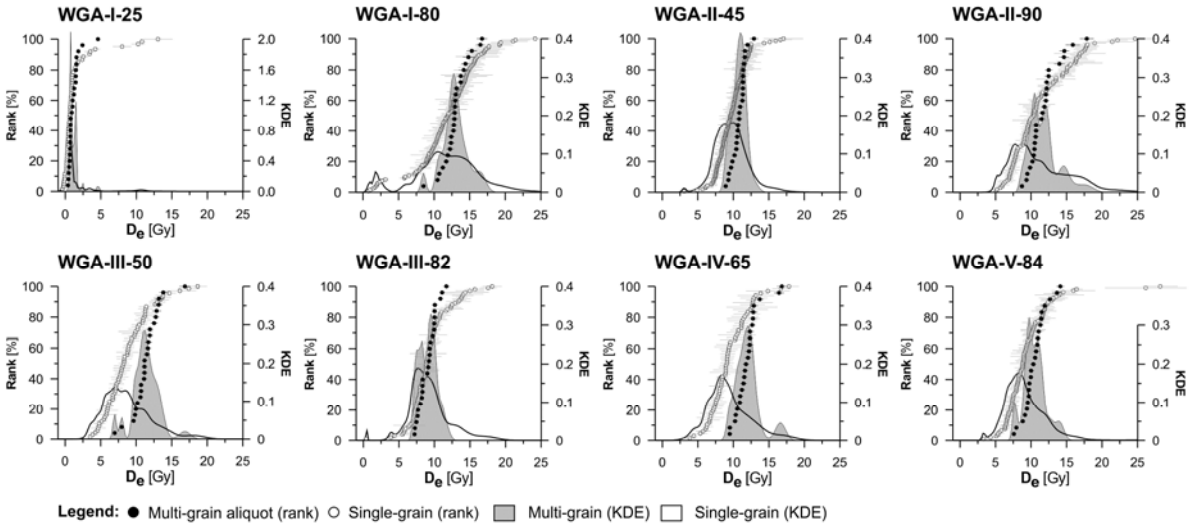

Fig. 5: Comparative age-rank and kernel-density-estimate (KDE) plots for D_e distributions from multi-grain aliquot and single-grain OSL analysis (closed circles, grey-shaded curve = multi-grain aliquots; open circles and white curve = single-grains).

3.4. Comparison of different dating approaches

OSL D_e and age data are summarized in STable 1 and Figure 6. The shape and overdispersion values of D_e distributions below WGA-I suggest to apply the CAM for both multi-grain aliquots and single-grains. While much of the chronology is generally stratigraphically consistent, it is clear that there is significant inter-approach variability. Multi-grain aliquot CAM D_e values and ages are an average of 20% (11–35%) larger than single-grain CAM D_e values and ages (SFig. 5). As problems with calibration of beta sources are ruled out (SFig. 2), this implies the presence of a proportion of grains with larger D_e values than the majority of grains as visible in the single-grain D_e distributions (Fig. 5, SFig. 3). These grains appear to affect the multi-grain aliquots D_es but are likely unrelated to partial bleaching during the depositional process, or post-depositional mixing (see above). In this context, it is important to note that the samples under consideration have a large amount of luminescent grains (SFig. 6), which will cause stronger averaging effects in the multi-grain aliquots compared to many other regions.

While the single-grain CAM ages appear to be reliable, they significantly overestimate the age control given by radiocarbon dating (Fig. 6). The charcoal and/or organic remains for radiocarbon dating were collected from discrete and undisturbed organic horizons making the possibility of significant mixing unlikely, and suggesting this chronology likely to be correct. Assuming that D_es in the lower portion of distributions may more accurately reflect depositional ages, we therefore apply the Minimum Age Model with 10 % overdispersion (MAM, Galbraith et al., 1999). For samples below the upper meter, single-grain MAM D_es are up to 53% lower than for the multi-grain CAM values (SFig. 5), and still up to 37% lower than for single-grain CAM values. Interestingly, single-grain MAM ages are generally consistent with radiocarbon ages (Fig. 6).

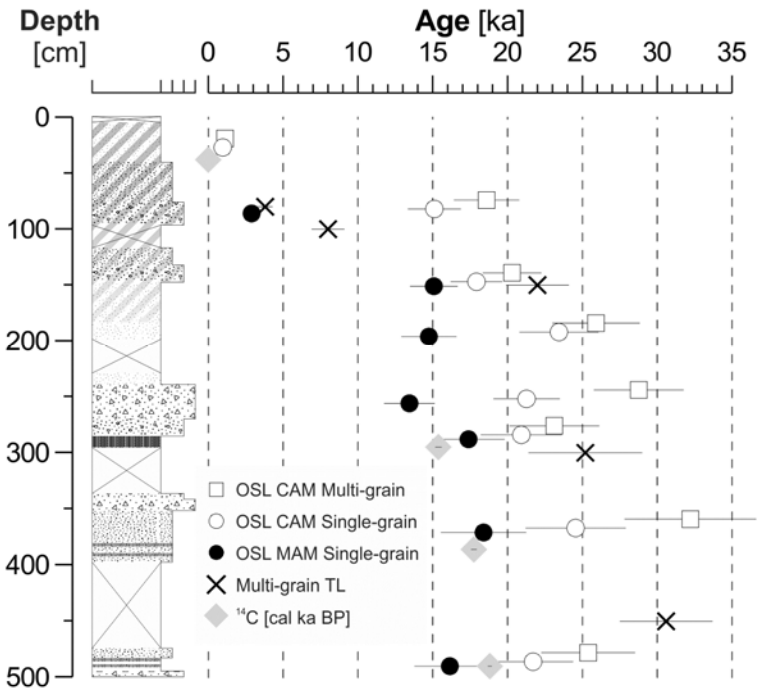

Fig. 6: Down-profile comparison of multi-grain aliquot luminescence techniques (TL as reported in Nott et al. 1996; and OSL CAM ages), single-grain OSL (CAM and MAM ages), and radiocarbon ages.

4. Discussion

Even though the TL signal generally bleaches more slowly than the OSL signal, our multi-grain aliquot OSL chronology is in good agreement with the existing TL chronology. In combination with the modern analogue samples this implies that both the TL and OSL signal were fully bleached prior to deposition. Potential problems for the TL chronology as highlighted by Nott et al. (1996) are unlikely to have significantly affected the originally published ages. Radioactive disequilibrium is shown to be minimal, and the low concentration of U, Th and K in the groundwater will not have a significant effect on dose rates. Sediment mixing is only significant in the uppermost meter. Nevertheless, these chronologies are inconsistent with radiocarbon dating, raising the question how the observed differences between chronologies can be explained.

In this context, thin sections revealed the presence of clay and iron rich (lateric) mud pellets (up to 0.5 counts per mm^2) and various heavy minerals (up to 0.38 counts per mm^2), both of which will have higher U, Th, and K contents than the surrounding quartz grains and thus act as micro-

dosimetric 'hot spots'. Therefore, quartz grains in proximity to these hot spots would have received a higher dose rate and, thus, accumulated dose faster than other grains. Mayya et al. (2006) have shown that beta dose inhomogeneity will cause positively skewed D_e distributions and suggest to use a minimum dose concept for D_e analyses. For the sediments investigated here, beta dose inhomogeneity is presumably mainly related to mud-pellets rich in clay (and hence K), whereas detrital zircon as mainly strong alpha emitter will have only a minor effect, as the outer part of the quartz grains has been removed by etching. However, zircon inclusions in quartz will have a strong effect on the internal dose rate of quartz that has been considered zero to this point. Furthermore, alpha emitters within quartz could change the OSL properties of the material with time by altering the structure of the crystal lattice and its point defects (Botis et al., 2005).

Given the low proportion of mud-pellets and heavy minerals, it is likely that the bulk dose rates as measured by high-resolution gamma spectroscopy more closely represent the dose rate received by grains away from 'hot spots' influence. In addition, each multi-grain aliquot (TL and OSL) will contain a mixture of grains that were adjacent to low-dose rate quartz and grains that were close to 'hot spot' material, thus yielding an averaged dose estimate. This is avoided by using single-grains. Also, the MAM will to some extent avoid the high doses caused by inclusions with the quartz. In combination this suggests that the single-grain MAM OSL chronology best accounts for the combined microdosimetric effects of mud-pellets and detrital heavy minerals, and likely reflects the deposition of these sediments most accurately - a conclusion that is supported by the radiocarbon chronology (Fig. 6).

5. Conclusions

Our multiple approach study suggests that (i) flood sediments in the levee sequence at Wangi Falls are generally characterised by good OSL properties, and (ii) there are no major problems related to the determination of the total dose rate, as mentioned by Nott et al. (1996). Furthermore, (iii) the

investigated fluvial sediments are likely not significantly affected by partial bleaching, as indicated by modern analogues. Nevertheless, we observe systematic differences between different luminescence techniques, which require additional explanations. Here, the presence of radiation 'hot spots' in the sediment and in particular within the grains is expected to significantly affect dose distributions. In order to account for the combined microdosimetric effects of mud pellets and heavy minerals, and in the absence of more detailed petrographic data as required for modelling, we consider that a MAM age estimate using the bulk measured dose rate will provide the closest possible estimate for the timing of deposition. This result is supported by the good consistency with radiocarbon dating. For flood sediments at Wangi Falls this suggests that the existing depositional chronology - and consequently the interpretation of large magnitude flooding during the LGM - needs to be reconsidered, with major implications for the interpretation of monsoon controlled fluvial dynamics in the terminal Pleistocene.

In conclusion, this example shows that even in the absence of more commonly reported problems related to OSL dating, the establishment of OSL based chronologies can be not straightforward and requires care. In particular the comparison of multi- and single-grain data in combination with microscopic inspection of the material is considered useful. So far, the effect of inclusions on internal dose rate has seen inappropriate consideration but will be required for generally improving the reliability of OSL dating.

Acknowledgements

The authors gratefully acknowledge all support by the Litchfield National Park team. Jenny Wolff is thanked for careful preparation of the OSL samples at Stockholm University, Nathan Jankowski is thanked for his help with thin section analysis, and Lily Yu and Helen Price facilitated the ICP-MS measurements. Gamma spectrometric measurements have been carried out by Detlev Degering at VKTA Rossendorf e.V., Germany. This study was funded by ARC Discovery Early Career Research Award (DP0987819) granted to JHM.

References

Ahmad, M., Wygralak, A.S., Ferenczi, P.A., Bajwah, Z.U., 1993. Explanatory Notes and Mineral Deposit Data Sheets - Pine Creek SD 52-8, in: Northern Territory Geological Survey (Ed.), 1:250.000 Metallogenic Map Series, Darwin.

Arnold, L., Roberts, R., Galbraith, R., DeLong, S., 2009. A revised burial dose estimation procedure for optical dating of youngand modern-age sediments. Quaternary Geochronology 4, 306-325.

Botis, S., Nokhrin, S.M., Pan, Y., Xu, Y., Bonli, T., Sopuck, V., 2005. Natural radiation-induced damage in quartz. I. Correlations between cathodoluminence colors and paramagnetic defects. The Canadian Mineralogist 43, 1565-1580.

Bøtter-Jensen, L., Andersen, C., Duller, G., Murray, A., 2003. Developments in radiation, stimulation and observation facilities in luminescence measurements. Radiation Measurements 37, 535-541.

Duller, G., 2003. Distinguishing quartz and feldspar in single grain luminescence measurements. Radiation Measurements 37, 161-165.

Galbraith, R.F., Roberts, R.G., Laslett, G.M., Yoshida, H., Olley, J.M., 1999. Optical Dating of Single and Multiple Grains of Quartz From Jinmium Rock Shelter, Northern Australia: Part I, Experimental Design and Statistical Models. Archaeometry 41, 339-364.

Hogg, A.G., Hua, Q., Blackwell, P.G., Niu, M., Buck, C.E., Guilderson, T.P., Heaton, T.J., Palmer, J.G., Reimer, P.J., Reimer, R.W., Turney, C.S.M., Zimmerman, S.R.H., 2013. SHCAL13 southern hemisphere calibration, 0–50,000 years cal BP. Radiocarbon 55, 1889-1903.

Mayya, Y.S., Morthekai, P., Murari, M.K., Singhvi, a.K., 2006. Towards quantifying beta microdosimetric effects in single-grain quartz dose distribution. Radiation Measurements 41, 1032-1039.

Murray, A.S., Wintle, A.G., 2000. Luminescence dating of quartz using an improved single-aliquot regenerative-dose protocol. Radiation Measurements 33, 57-73.

Nott, J., Price, D., 1999. Waterfalls, floods and climate change: evidence from tropical Australia. Earth and Planetary Science Letters 171, 267-276.

Nott, J.F., Price, D.M., Bryant, E.A., 1996. A 30,000 year record of extreme floods in tropical Australia from relict plunge-pool deposits: Implications for future climate change. Geophysical Research Letters 23, 379-382.

Prescott, J., Hutton, J.T., 1994. Cosmic ray contributions to dose rates for luminescence and ESR dating: large depths and long-term time variations. Radiation Measurements 23, 497-500.

Preusser, F., Degering, D., 2007. Luminescence dating of the Niederweningen mammoth site, Switzerland. Quaternary International 164, 106-112.

Preusser, F., Kasper, H.U., 2001. Comparison of dose rate determination using high-resolution gamma spectrometry and inductively coupled plasma-mass spectrometry. Ancient TL 19, 19-23.

Reeves, J.M., Bostock, H.C., Ayliffe, L.K., Barrows, T.T., De Deckker, P., Devriendt, L.S., Dunbar, G.B., Drysdale, R.N., Fitzsimmons, K.E., Gagan, M.K., Griffiths, M.L., Haberle, S.G., Jansen, J.D., Krause, C., Lewis, S., McGregor, H.V., Mooney, S.D., Moss, P., Nanson, G.C., Purcell, A., van der Kaars, S., 2013. Palaeoenvironmental change in tropical Australasia over the last 30,000 years – a synthesis by the OZ-INTIMATE group. Quaternary Science Reviews 74, 97-114.

Richter, D., Richter, A., Dornich, K., 2013. Lexsyg—A new system for luminescence research. Geochronometria 40, 220-228.

Stuiver, M., Reimer, P.J., 1993. Extended 14C database and revised CALIB radiocarbon calibration program. Radiocarbon 35, 215-230.

Zander, A., Degering, D., Preusser, F., Kasper, H.U., Brückner, H., 2007. Optically stimulated luminescence dating of sublittoral and intertidal sediments from Dubai, UAE: Radioactive disequilibria in the uranium decay series. Quaternary Geochronology 2, 123-128.

Appendix A. Supplementary data

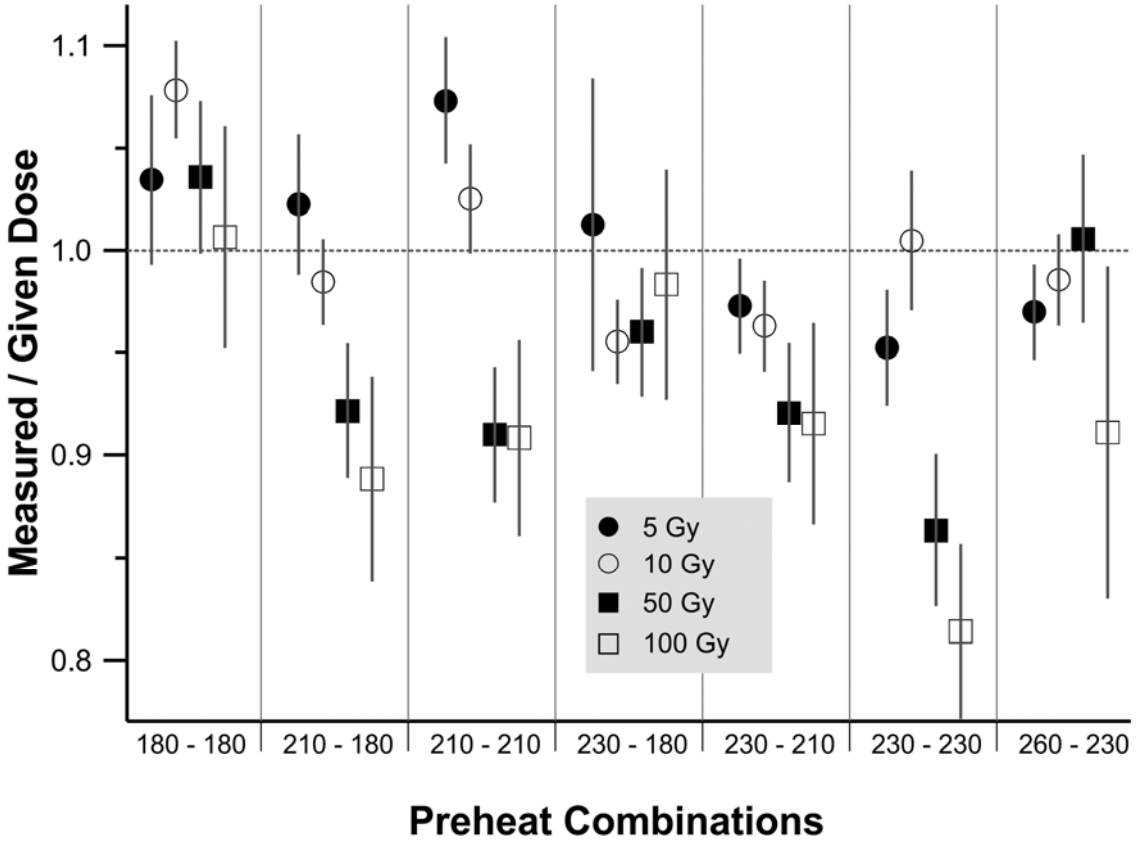

SFig. 1: Results from dose recovery experiments on 2 mm multi-grain aliquots with varying given doses (5, 10, 50, 100 Gy) and preheat combinations (note: errors are 2σ).

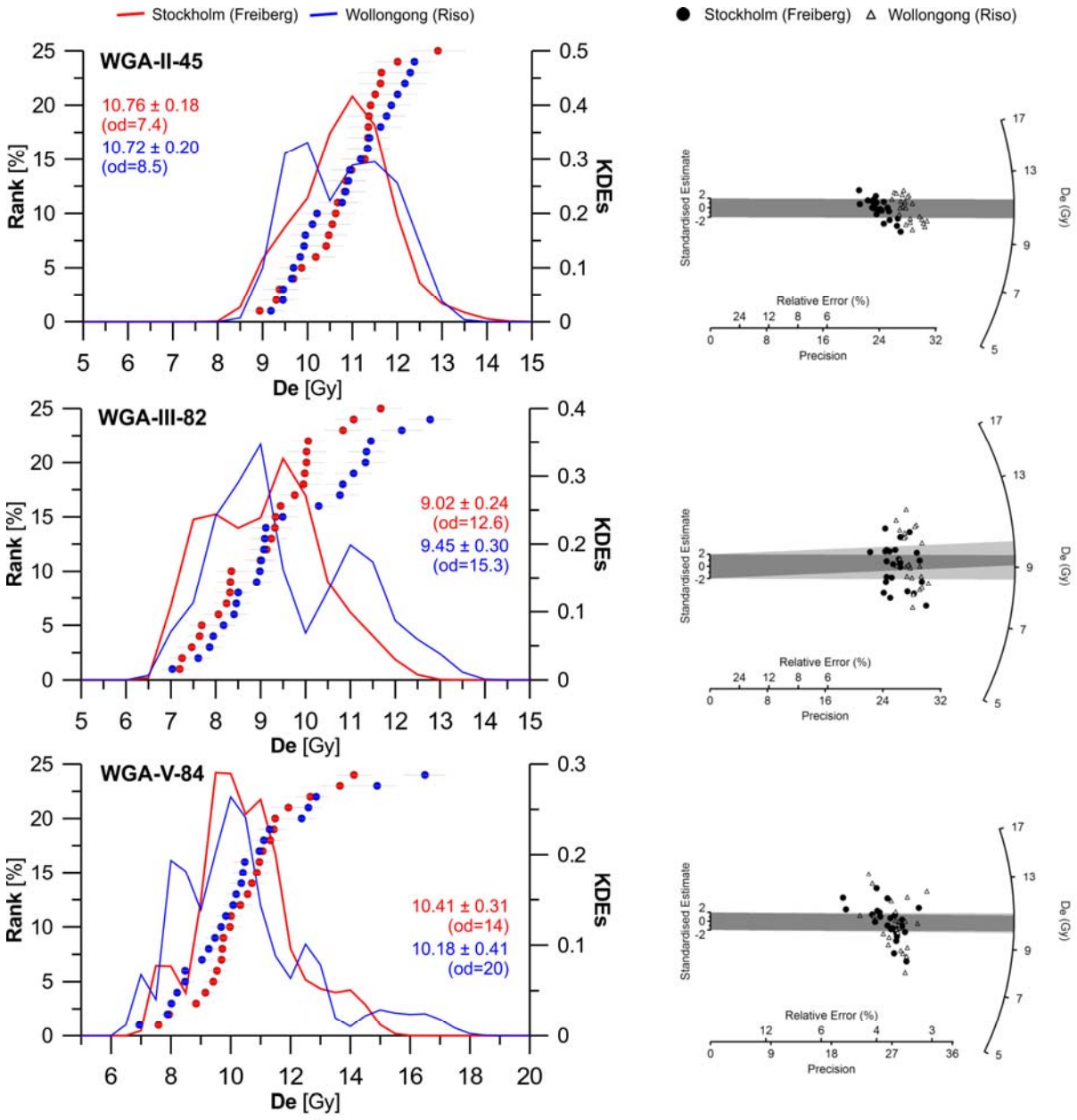

SFig. 2: Inter-laboratory comparison showing excellent agreement between measurements at Stockholm University (Freiberg Instruments Lexsyg Research reader) and the University of Wollongong (Risø TL/OSL-DA-20).

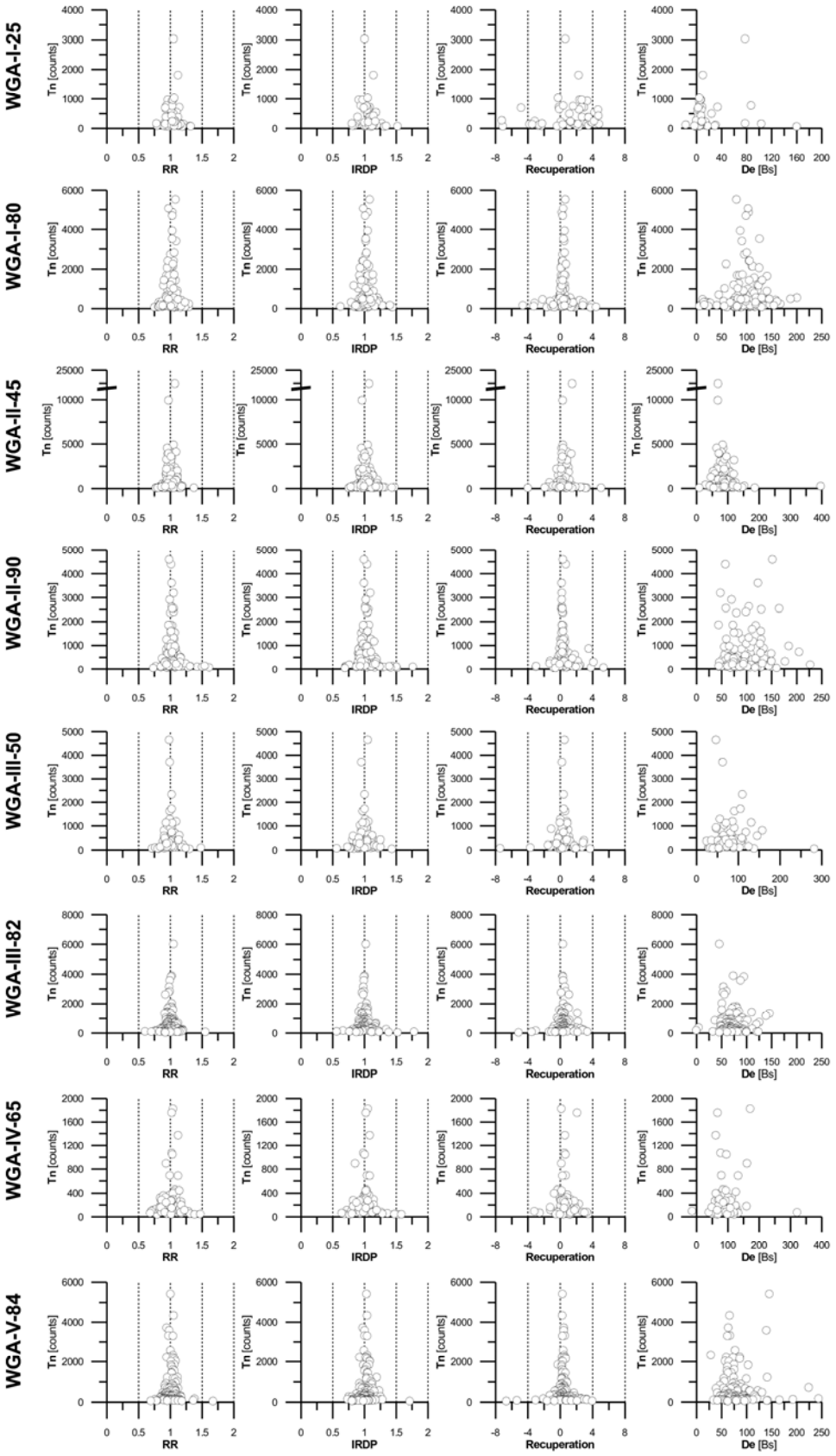

SFig. 3: Recycling ratios, IR depletion ratios, recuperation ratios, and relationship between D_e and natural test dose counts (i.e., brightness) for all accepted single-grain WGA samples.

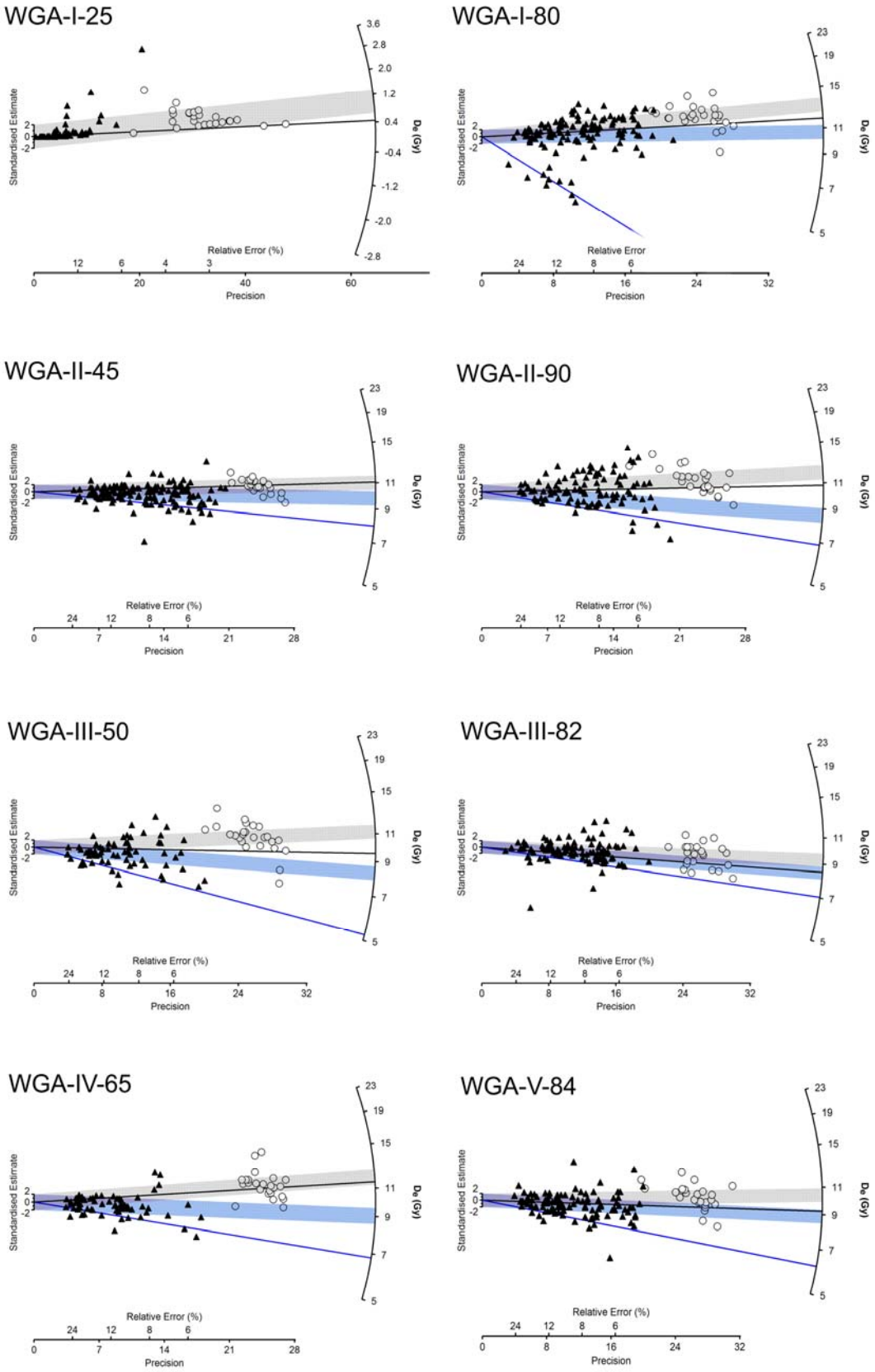

SFig. 4: Radialplots for all WGA single-grain (triangles) and multi-grain (circles) D_e distributions (grey bars are 2σ multi-grain CAM estimates, blue bars are 2σ single-grain CAM estimates).

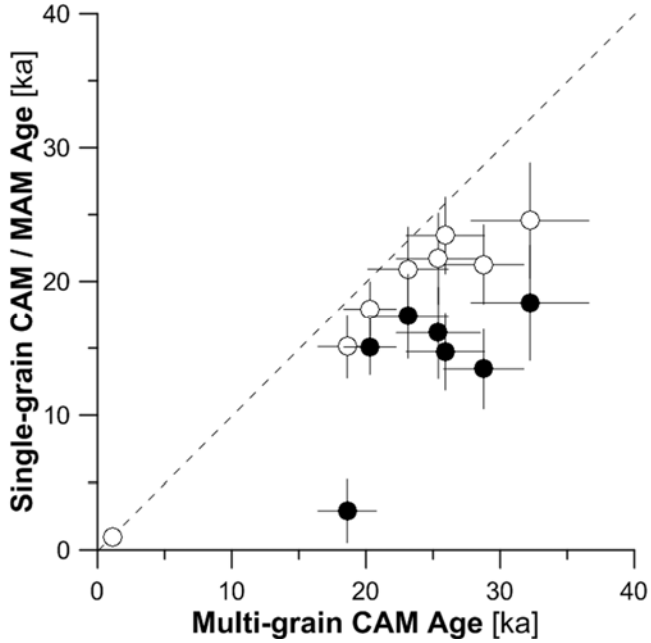

SFig. 5: Comparison between multi-grain CAM ages and single-grain CAM (white circles) and MAM (black circles) ages for all WGA samples.

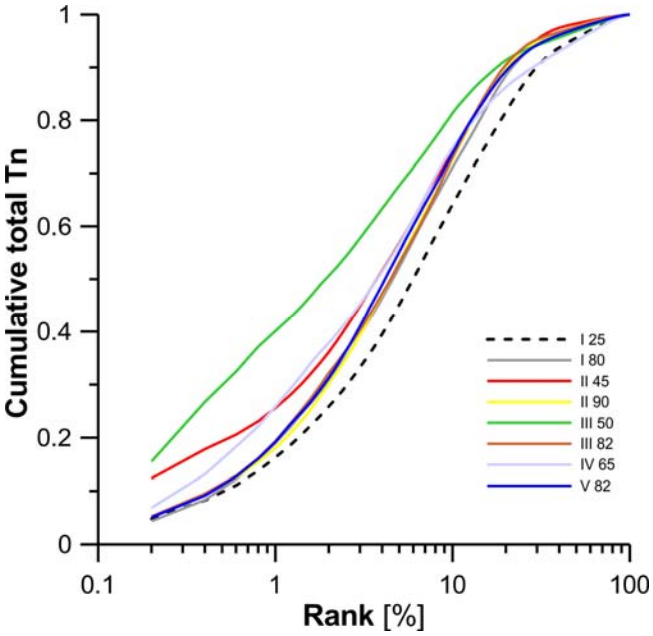

SFig. 6: Single-grain light-sum curves showing that a larger number of grains from Wangi Falls is emitting OSL than found in most other sediments.

STable 1: Results from multi-grain and single-grain OSL dating

Sample	Depth [cm]	Multi-grain Aliquots						Single grains									
		n	od.	CAM D_e [Gy]	±	Age [ka]	±	n	od.	CAM D_e [Gy]	±	Age [ka]	±	MAM[1] D_e [Gy]	±	Age [ka]	±
WG-BAR	-	24	-	0.24	0.08	-	-	93	-	0.019[3]	0.002	-	-	-	-	-	-
WGA-552	-	24	-	0.10	0.03	-	-	61	-	0.150[3]	0.760	-	-	-	-	-	-
WGA-I-25	25	25	0.57	0.98	0.11	1.11	0.17	61	0.12	0.85	0.12	0.96	0.10	-	-	-	-
WGA-I-80	80	25	0.14	12.83	0.37	18.5	2.2	120	0.57	10.42	0.56	15.11	1.78	2.00	0.17	2.89	0.42
WGA-II-45[2]	145	25	0.07	10.76	0.18	20.2	2.0	140	0.20	9.50	0.18	17.92	1.73	7.68	0.25	15.07	1.60
WGA-II-90	190	25	0.16	11.66	0.39	25.7	2.8	104	0.33	10.55	0.36	23.43	2.65	6.63	0.36	14.74	1.85
WGA-III-50	250	25	0.17	11.22	0.39	28.5	3.3	68	0.34	8.30	0.36	21.27	2.22	5.24	0.37	13.44	1.69
WGA-III-82[2]	282	25	0.13	9.02	0.24	23.1	2.8	102	0.36	8.16	0.30	20.92	2.71	6.78	0.34	17.39	2.42
WGA-IV-65	365	24	0.13	11.92	0.34	32.3	4.1	67	0.25	9.08	0.32	24.55	3.35	6.81	0.50	18.39	2.85
WGA-V-84[2]	484	24	0.14	10.41	0.31	25.6	3.0	107	0.28	8.90	0.26	21.70	2.68	6.17	0.27	16.14	2.38

1 MAM3 (Galbraith et al., 1999)

2 Outlier D_es removed

3 unlogged-CAM (Arnold et al., 2009)

STable 2: Detailed statistics for single-grain selection criteria

Sample	Depth [cm]	# of grains	Failed Criterion 1	Failed Criterion 2	Failed Criterion 3	Failed Criterion 4	Failed Criterion 5	Failed for other reasons*	Total accepted grains	% grains accepted	Rej / Acc
WGA-I-25	25	500	297	135	180	177	234	3	61	12	7.20
WGA-I-80	80	500	290	138	187	191	154	1	120	24	3.17
WGA-II-45	145	500	281	116	180	169	144	6	140	28	2.57
WGA-II-90	190	500	308	127	189	201	154	8	104	21	3.81
WGA-III-50	250	500	350	143	202	238	195	6	68	14	6.35
WGA-III-82	282	500	314	121	201	201	164	3	102	20	3.90
WGA-IV-65	365	500	369	171	220	229	154	6	67	13	6.46
WGA-V-84	484	500	306	141	191	195	158	5	107	21	3.67

Criterion 1 (basis: test dose in NATURAL:TN>3xBG)

Criterion 2 (basis: test dose error in NATURAL: TN error >20%)

Criterion 3 (basis: recycling ratio: >2s from unity)

Criterion 4 (basis: IRD ratio: >2s from unity)

Criterion 5 (basis: recuperation: zero Lx/Tx >5% of Ln/Tn)

*for other reasons, i.e., fast ratio, no Ln/Tn

STable 3: Results from high-resolution gamma spectrometry and the resulting total dose rates for WGA samples and three bedrock samples from the Wangi Creek catchment

Sample	**Depth**	**^{238}U**	±	**^{226}Ra**	±	**^{210}Pb**	±	**^{232}Th**	±	**^{228}Ra**	±	**^{228}Th**	±	**^{40}K**	±	**^{137}Cs**	**U**	±	**Th**	±	**K**	±	**D**
	cm	[Bq/kg]	1* s	[Bq/kg]	1* s	[Bq/kg]	1* s	[Bq/kg]	1* s	[Bq/kg]	1* s	[Bq/kg]	1* s	[Bq/kg]	1* s	[Bq/kg]	[ppm]	1* s	[ppm]	1* s	[%]	1* s	(Gy ka-1)
WGA-I-25±5	25	17.10	1.80	14.30	0.80	11.10	1.40	18.90	0.90	17.50	1.20	19.20	0.90	23.40	2.80	0.57	1.39	0.14	4.66	0.22	0.08	0.01	0.88 ± 0.09
WGA-I-80±5	80	12.40	1.90	11.70	0.60	12.40	1.50	13.90	0.70	14.50	1.00	13.80	0.70	19.90	2.20	0.45	1.01	0.15	3.43	0.18	0.06	0.01	0.69 ± 0.08
WGA-II-45±5	145	9.40	0.90	7.20	0.40	7.10	0.70	9.40	0.40	10.00	0.60	9.30	0.40	15.00	1.10	0.19	0.76	0.07	2.32	0.11	0.05	0.00	0.53 ± 0.05
WGA-II-90±5	190	8.20	0.80	5.60	0.30	6.40	0.60	7.50	0.40	7.60	0.50	7.40	0.40	9.60	1.20	0.21	0.66	0.07	1.84	0.09	0.03	0.00	0.45 ± 0.05
WGA-III-50±5	250	5.40	0.70	5.50	0.30	7.50	0.70	8.00	0.40	8.30	0.60	8.00	0.40	7.60	1.30	0.26	0.43	0.06	1.98	0.10	0.03	0.00	0.39 ± 0.04
WGA-III-82±8	282	6.10	0.90	5.90	0.30	8.10	0.80	7.70	0.40	7.70	0.60	7.70	0.40	5.50	0.90	0.24	0.49	0.08	1.91	0.10	0.02	0.00	0.39 ± 0.05
WGA-IV-65±5	365	6.30	1.00	5.50	0.30	7.90	0.90	7.00	0.40	7.10	0.60	7.00	0.40	5.10	1.30	0.30	0.51	0.08	1.73	0.10	0.02	0.00	0.37 ± 0.05
WGA-V-84±6	484	7.50	0.90	6.40	0.40	7.00	1.00	8.10	0.40	8.60	0.70	7.90	0.40	10.90	1.30	0.29	0.61	0.08	1.99	0.11	0.04	0.00	0.41 ± 0.05
WG Laterite	-	90.07	9.01	82.15	4.76	83.03	9.96	59.48	3.45	59.41	4.22	59.50	3.81	23.82	4.76	1.59	7.29	0.73	14.66	0.85	0.08	0.02	-
WG Sandstone	-	5.08	1.02	4.04	0.29	18.22	1.82	6.50	0.44	6.30	0.52	6.55	0.45	17.48	1.92	1.05	0.41	0.08	1.60	0.11	0.06	0.01	-
WG Quartzite	-	5.54	1.33	6.26	0.46	8.75	1.49	6.46	0.46	6.05	0.60	6.54	0.47	3.60	1.08	1.19	0.45	0.11	1.59	0.11	0.01	0.00	-

STable 4: Results from thin section analysis by point counting.

Sample	Depth	Quartz	Clay Pellets	Heavy Minerals	Charcoal	Void
		[counts/mm2]	[counts/mm2]	[counts/mm2]	[counts/mm2]	[counts/mm2]
WGA-I-64	64	29.38	0.00	0.38	0.15	31.62
WGA-II-64	164	31.69	0.19	0.12	0.23	29.31
WGA-III-99	299	32.27	0.23	0.23	1.00	27.81
WGA-IV-78	378	35.58	0.35	0.04	0.00	25.58
WGA-V-63	463	39.46	0.50	0.04	0.04	21.50

STable 5: Results radiocarbon dating.

Sample	Depth [cm]	Lab Code	Material	^{13}C/^{12}C	Conventional Age [^{14}C yr BP / *pMC*]	Calibrated Age[1] 2σ [cal yr BP]
WGA-I-36-40	38	WK 39269	Charcoal	n.a.	*103.2 ± 0.3*	modern
WGA-III-92-99	95	Beta 340459	Organic Remains	-19.7	12910 ± 50	15160 - 15596
WGA-IV-84-87	86	Beta 340460	Charcoal	n.a.	14610 ± 60	17554 - 17947
WGA-V-90	90	Beta 340461	Organic Remains	-24.1	15610 ± 60	18675 - 18954

1 using Calib 7.0 and SHcal13 calibration curve (see text for details)

STable 6: Results from ICP-MS measurements on water samples.

Sample	K [ppb]	Th [ppb]	U [ppb]
WG 437	< 200	< 0.08	< 0.06
WG-FALL	< 200	< 0.02	< 0.01